Article

Evaluation of Biomedical Ti/ZrO$_2$ Joint Brazed with Pure Au Filler: Microstructure and Mechanical Properties

Yuzhen Lei [1,2], Hong Bian [1,2,*], Wei Fu [1,2], Xiaoguo Song [1,2], Jicai Feng [1,2], Weimin Long [3] and Hongwei Niu [2,4]

1   State Key Laboratory of Advanced Welding and Joining, Harbin Institute of Technology, Harbin 150001, China; lei.yuzhen@163.com (Y.L.); fuwei_drmf@126.com (W.F.); xgsong@hitwh.edu.cn (X.S.); feng_jicai@163.com (J.F.)
2   Shandong Provincial Key Lab of Special Welding Technology, Harbin Institute of Technology at Weihai, Weihai 264209, China; niuhongwei7788@sina.com
3   State Key Laboratory of New Brazing Materials and Technology, Zhengzhou Research Institute of Mechanical Engineering Co., Ltd., Zhengzhou 450001, China; brazelong@163.com
4   Shandong Institute of Shipbuilding Technology, Weihai 264209, China
*   Correspondence: whenstreaming163@163.com; Tel.: +86-631-5678454

Abstract: Titanium and zirconia (ZrO$_2$) ceramics are widely used in biomedical fields. This study aims to achieve reliable brazed joints of titanium/ZrO$_2$ using biocompatible Au filler for implantable medical products. The effects of brazing temperature and holding time on the interfacial microstructures and mechanical properties of titanium/Au/ZrO$_2$ joints were fully investigated by scanning electron microscopy (SEM), energy-dispersive spectrometry (EDS) and X-ray diffraction (XRD). The results indicated that the typical interfacial microstructure of the titanium/Au/ZrO$_2$ joint was titanium/Ti$_3$Au layer/TiAu layer/TiAu$_2$ layer/TiAu$_4$ layer/TiO layer/ZrO$_2$ ceramic. With an increasing brazing temperature or holding time, the thickness of the Ti$_3$Au + TiAu + TiAu$_2$ layer increased gradually. The growth of the TiO layer was observed, which promoted metallurgical bonding between the filler metal and ZrO$_2$ ceramic. The optimal shear strength of ~35.0 MPa was obtained at 1150 °C for 10 min. SEM characterization revealed that cracks initiated and propagated along the interface of TiAu$_2$ and TiAu$_4$ reaction layers.

Keywords: biomedical titanium; zirconia bioceramic; brazing; interfacial microstructure; mechanical properties

1. Introduction

As one of the most popular biomedical metallic materials, titanium and titanium alloys have been widely used to produce bone trauma products, artificial joints, cardiovascular stents, dental implants and other medical products, owing to their low density, low elastic modulus, non-toxic behavior, good corrosion resistance and excellent biocompatibility [1–8]. In recent decades, the production and application of zirconia bioceramics have developed rapidly. The properties that it processes, such as its high hardness, high wear resistance, excellent biocompatibility and aesthetic effect make it suitable for surgical implant fabrication, especially for implants in the field of prosthodontics [9–13]. In many applications, metal–ceramic hybrid components are desired for the manufacturing of implantable medical products—for example, dental implants, micro-stimulators and so on [14–16].

At present, the main joining methods for metal–ceramic components in implant manufacturing are cementation and mechanical bonding [17–20]. However, the joints of metal–ceramic composites

constructed via these bonding methods display a low strength and are easy to loosen in practice, which can shorten the life of implants and lead to potential dangers in applications. Brazing, a bonding technology with the advantages of convenience, cost-effectiveness and high quality, has been widely employed for joining metals and ceramics [21–23]. Sharma et al. [24,25] realized the brazing of Ti-6Al-4V to ZrO_2 successfully using Ag-Cu-In-Ti active filler and Ag-Cu-Ti composite fillers. ZrO_2 was boned under the influence of active Ti from filler, which was absorbed in the surface pores through capillary action at the ZrO_2 surface. Fu et al. [26] and Bian et al. [27,28] used Sn-Ti and SnAgCu-Ti active fillers to achieve the bonding of zirconia ceramics. The TiO_x compounds were observed on the ZrO_2 side. Smorygo et al. [16] used Cu-Ag-Ti filler to achieve the bonding of titanium to a zirconia ceramic by forming a layer of TiO_x with a thickness of 3–4 μm between the filler and ZrO_2 sample. Moreover, the authors pointed out that the brazing temperature and holding time had great influences on the evolution of the bond layer microstructure and the fracture behavior. Feng et al. [29] and Dai et al. [30] utilized AgCu and AgCu composite fillers to achieve the bonding of a titanium alloy to a zirconia ceramic. The Ti from the substrates crossed the brazing seam, accumulated on the ZrO_2 and reacted with the ZrO_2 to form a TiO layer. In other words, the key to obtaining reliable bonding is the formation of Ti-O compounds adjacent to the ceramics. There are two main ways for Ti to form Ti-O reported in the literature, namely by adding Ti into the filler metal and by diffusing it from the base metal. The issue is that the fillers that are usually used to braze metal and ceramics mainly contain toxic elements, making them unsuitable for use in the bonding of biomedical joints. One potential solution is to use Au, a biocompatible element, as the filler metal [31–36]. In addition, the melting point of Au is much lower than that of titanium and zirconia ceramics, and its ductility is high, which is conducive to the stress relief of metal–ceramic brazed joints. Furthermore, according to the binary alloy phase diagram of Ti-Au [37], Ti can react with Au. Thus, when adopting pure Au as the filler to bond titanium or titanium alloys to ceramics with appropriate brazing parameters, Ti can cross the brazing seam to react with ceramics and realize the bonding of titanium or titanium to ceramics. Bian et al. [38] adopted Au foil to braze titanium and alumina ceramic and a good brazed joint was successfully obtained for implantable devices, where the formation of a Ti–O layer adjacent to alumina was deduced but not definitely identified. Up to now, studies on brazing metals and ceramics for biomedical applications are still rare.

In this study, the reliable brazing of biomedical titanium to zirconia ceramic was achieved by adopting biocompatible Au filler. The typical microstructure of the brazed joints was analyzed. Detailed investigations into the effects of brazing temperature and holding time on the microstructural evolution, Ti–O compound layer and mechanical properties were conducted. The shear strength of joints was tested, and fracture analyses were conducted to understand the mechanisms of the fractures.

2. Experimental Materials and Methods

Commercial pure titanium of purity 99.6 wt.%, mainly doped with 0.2 wt.% Fe and 0.18 wt.% O, provided by Kunshan Bitaita Metal Products Co., Ltd., Kunshan, China, was cut into 20 mm × 10 mm × 2 mm pieces. Figure 1a,b shows the microstructure and XRD pattern of pure titanium (according to PDF#00-044-1294), respectively. It was clearly seen that the pure titanium mainly consisted of α-Ti with an equiaxed structure. Sintered 3 mol% yttria-stabilized zirconia, supplied by Shanghai Unite Technology Co., Ltd., Shanghai, China, was cut into 5 mm cubes using a diamond cutter. The back-scattered electron (BSE) image of ZrO_2 was shown in Figure 1c. Au foil with a purity of 99.99% and thickness of 50 μm, which was used in the experiment, was supplied by KYKY Technology Co., Ltd., Beijing, China.

Prior to vacuum brazing, the surface of the titanium to be brazed was ground to a grit of 3000 mesh by SiC grinding paper. Both substrates and the Au foil were cleaned using an ultrasonic bath in acetone for 15 min, followed by air blowing. Then, the Au foils were sandwiched between the substrates, as shown in Figure 1d. Brazing was performed in a vacuum furnace with a vacuum of 1.3×10^{-3} Pa. The assembly was firstly heated to 1000 °C for 10 min from an ambient temperature, at a heating rate of 20 °C/min, and then two groups of experiments were designed in order to investigate the effects

of brazing temperature and holding time on the microstructures and mechanical properties of the brazed joints: in one experiment, the temperature continued to increase to the brazing temperature (1110–1190 °C) at a rate of 10 °C/min, with the holding time fixed at 10 min; in the other set of experiments, the temperature continued to increase to 1150 °C at a rate of 10 °C/min, with the holding time varying from 5 to 30 min. Subsequently, the specimens were cooled down to 300 °C at a rate of 5 °C/min. Finally, the assembly was spontaneously cooled to room temperature in the furnace.
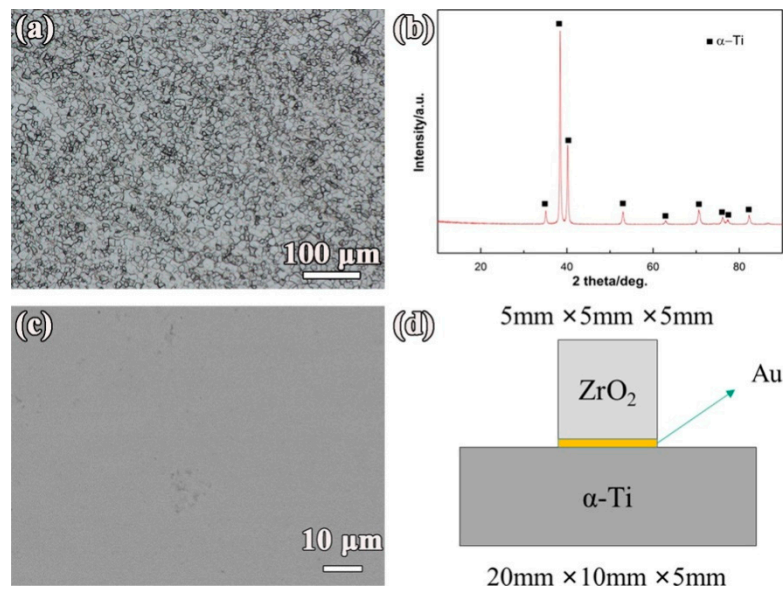

Figure 1. Microstructures of substrates and schematic diagram of brazing assembly. (**a**) Metallographic figure of α-Ti alloy, (**b**) XRD pattern of α-Ti alloy, (**c**) BSE image of ZrO_2 ceramic and (**d**) brazing assembly.

After the experiments, the cross-sections of brazed joints, which were obtained by cutting the specimens perpendicular to the brazed interface using a diamond saw, were polished for microstructural observations, and they were characterized with an SEM (MERLIN Compact, ZEISS, Stuttgart, Germany) in BSE mode, equipped with an EDS (Octane Plus, EDAX, Mahwah, NJ, USA) to analyze the composition of various reaction phases. The shear tests were performed with a universal testing machine (Instron 5967, Instron, Boston, MA, USA) at a constant rate of 1 mm/min at room temperature. The experimental data were averaged from at least five specimens after removing the outliers for each parameter. After the shear test, three randomly selected fractured specimens were analyzed by SEM in BSE mode and XRD (DX-2700, Dandong Haoyuan Instrument Co., Ltd., Dandong, China), equipped with Cu-Kα (λ = 0.154 nm), at operating parameters of 40 KV and 30 mA to identify the fracture path.

3. Results and Discussion

3.1. Typical Interfacial Microstructure of Titanium/Au/ZrO₂ Joint

Figure 2 showed the typical microstructure and the main element distribution of the titanium/Au/ZrO₂ joint brazed at 1150 °C for 10 min. As shown in Figure 2a–b, a sound joint without any microcracks or pores was obtained, and the joint could be divided into five zones based on its different microscopic morphologies. According to the elemental distribution along the red line shown in Figure 2c, it can be seen that the content of Ti decreased gradually from the titanium substrate to the ZrO_2 ceramic, while an opposite trend for Au was observed. It was worth noting that there were four platforms in the variation curve of both Ti and Au elements, which corresponded to Zones I, II, III and IV in Figure 2b. Combined with the elemental distribution maps in Figure 2d–g, it was deduced that Ti dissolved and diffused to the molten Au. At the same time, Au also diffused to the Ti substrate. From the phase diagram of Au-Ti [37], it can be seen that Ti and Au form Ti_xAu_y intermetallic compounds (IMCs) easily. In addition, the diffusion

of Ti across the brazing seam occurred, with Ti segregation on the ZrO_2 ceramic side also observed, forming Ti-O compounds via the following reaction: $Ti + ZrO_2 \rightarrow TiO_x + ZrO_{2-x}$ [39–41]. Eventually, Zone V was formed via metallurgical bonding between the filler metal and the ceramic.
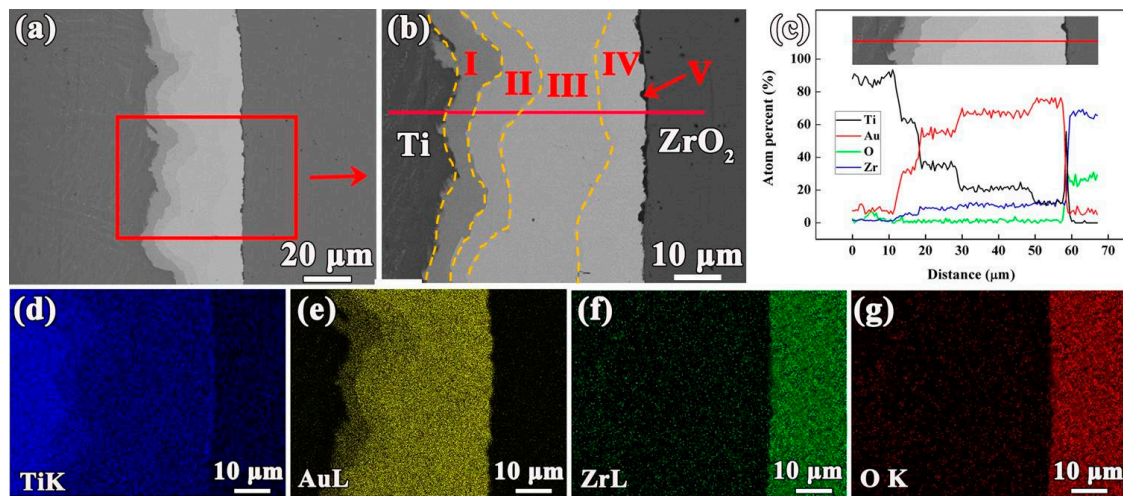

Figure 2. Typical microstructures and elemental distribution of titanium/Au/ZrO_2 joint at 1150 °C for 10 min: (**a**) lower and (**b**) higher magnification of the typical interfacial microstructure, (**c**) line distributions and (**d**–**g**) map distributions of Ti, Au, Zr and O.

In order to reveal more details of each zone in the titanium/Au/ZrO_2 joint, the highly magnified interfacial microstructures of Zones I–V are shown in Figure 3. The EDS chemical compositions of each spot in Figure 3 are listed in Table 1. The EDS analyses of Zones I–IV showed that these zones mainly contained Ti and Au. According to the molar ratio of Ti/Au and the Ti-Au binary phase diagram [37], it can be concluded that the zones from I to VI were Ti_3Au phase (Spot A), TiAu phase (Spot B), $TiAu_2$ phase (Spot C) and $TiAu_4$ phase (Spot D), respectively. When the brazing temperature exceeded the melting point of Au (1064 °C), the Au foil began to melt and the interdiffusion of Ti and Au occurred, both of which were driven by the concentration gradient. Then, Ti reacted with Au to form Ti_3Au, TiAu, $TiAu_2$ and $TiAu_4$ IMCs due to the decreasing concentration gradient of Ti [38]. Through the cooling process, the Ti_3Au, TiAu, $TiAu_2$ and $TiAu_4$ layers formed. The thicknesses of these layers, on average, were ~4.8 μm, 5.3 μm, 14.2 μm and 10.2 μm combined with Figure 2a–b. The chemical composition of Spot E in Zone V detected by EDS analysis showed that the titanium/oxygen atomic ratio was about 1:1. Combined with the results of Ti reacting with ZrO_2 ceramics in previous studies [42,43], it can be deduced that the black layer (Zone V) next to the ZrO_2 side was a TiO layer. Therefore, the active Ti from the substrate had two effects during brazing: one was to react with Au to form Ti–Au compounds, and the other was to react with the ZrO_2 ceramic to form a metallurgical bond.
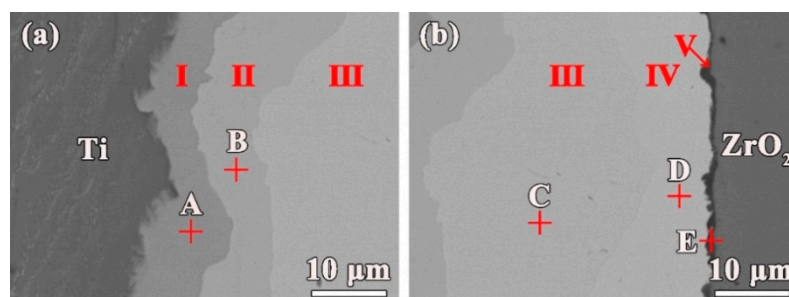

Figure 3. Magnification microstructure of the titanium/Au/ZrO_2 joint: (**a**) the titanium/brazing seam interface; (**b**) the brazing seam/ZrO_2 interface.

Table 1. Energy dispersive spectroscopy (EDS) results of the spots marked in Figure 3 (at.%).

Spot	Ti	Au	Zr	O	Possible Phases
A	75.67	22.48	0.02	1.83	Ti_3Au
B	49.60	47.67	0.06	2.67	$TiAu$
C	32.05	61.52	0.03	6.40	$TiAu_2$
D	18.44	73.80	0.04	7.72	$TiAu_4$
E	40.29	2.07	3.02	54.62	TiO

Based on the above analyses, it can be concluded that the representative brazing microstructure of the titanium/Au/ZrO_2 joint brazed at 1150 °C for 10 min was titanium/Ti_3Au layer/TiAu layer /$TiAu_2$ layer /$TiAu_4$ layer /TiO layer /ZrO_2 ceramic.

3.2. Effects of Brazing Parameters on the Interfacial Microstructure of the Titanium/Au/ZrO_2 Joints

It is acknowledged that the brazing temperature plays an important role in the evolution of interfacial microstructure [16,29]. The microstructural evolutions of brazed joints at 1110–1190 °C at intervals of 20 °C are shown in Figure 4a–e. It can be seen that the zones and phases in the joints are consistent with the typical interfacial microstructure. However, with a rise in the brazing temperature, the thickness of $Ti_3Au+TiAu+TiAu_2$ layers increased gradually from 19.2 μm to 24.3μm, owing to the enhanced diffusion of Ti and Au with the increasing temperature, as shown in Figure 4a–c. With the brazing temperature increasing further, as shown in Figure 4d–e, the thickness of $Ti_3Au + TiAu + TiAu_2$ layers showed no obvious change due to the Ti–Au reaction layers hindering the further diffusion of Ti and Au by acting as barriers.
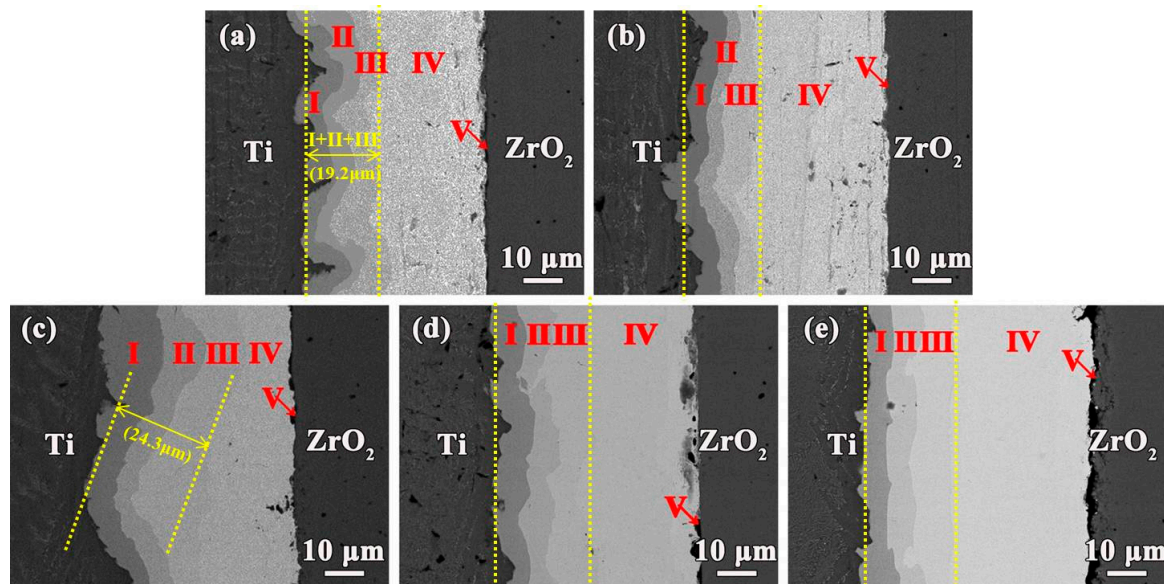

Figure 4. Microstructure of the titanium/Au/ZrO_2 joint brazed at different brazing temperatures for 10 min: (**a**) 1110 °C, (**b**) 1130 °C, (**c**) 1150 °C, (**d**) 1170 °C and (**e**) 1190 °C.

In order to further analyze the microstructural evolutions of the TiO layer in the titanium/Au/ZrO_2 joint, the highly magnified microstructures of Zone V are shown in Figure 5. When the brazing temperature was low (e.g., 1110 °C), only a limited number of Ti atoms diffused to the ZrO_2 surface and reacted with O atoms from ZrO_2 to form a thin layer of TiO, which was not obviously observed by SEM, as shown in Figure 5a. With the increase in temperature, more sufficient Ti atoms diffused to and

accumulated on the ZrO_2 surface. Thus, the thickness of the TiO layers increased gradually, as shown in Figure 5b–e.
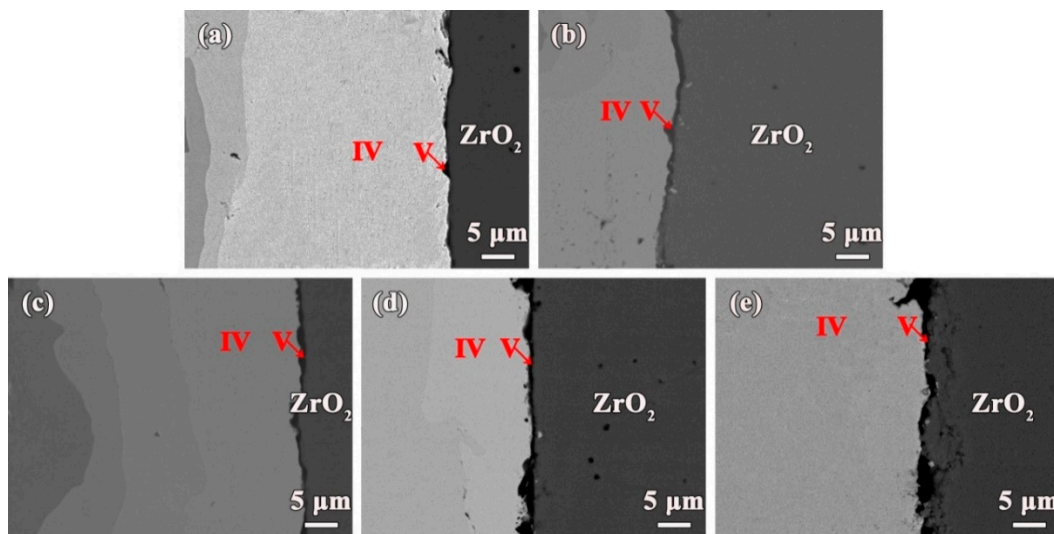

Figure 5. Microstructure of the TiO layer at different brazing temperature for 10 min: (**a**) 1110 °C, (**b**) 1130 °C, (**c**) 1150 °C, (**d**) 1170 °C and (**e**) 1190 °C.

It was well known that holding time is the other important factor affecting brazing quality, besides brazing temperature. Figure 6a–e showed the BSE images of the interfacial microstructure of the titanium/Au/ZrO_2 joint brazed at 1150 °C for 5–30 min, respectively. Notably, the joints still consisted of five zones and the phases were consistent with the typical interfacial microstructure shown in Figure 2. With a longer holding time, the diffusion of Ti atoms was more sufficient and the thickness of Ti_3Au + TiAu + $TiAu_2$ layers increased gradually from 22.6 µm to 30.3 µm. Additionally, the TiO layer showed no significant changes, except for a slight increase in thickness.
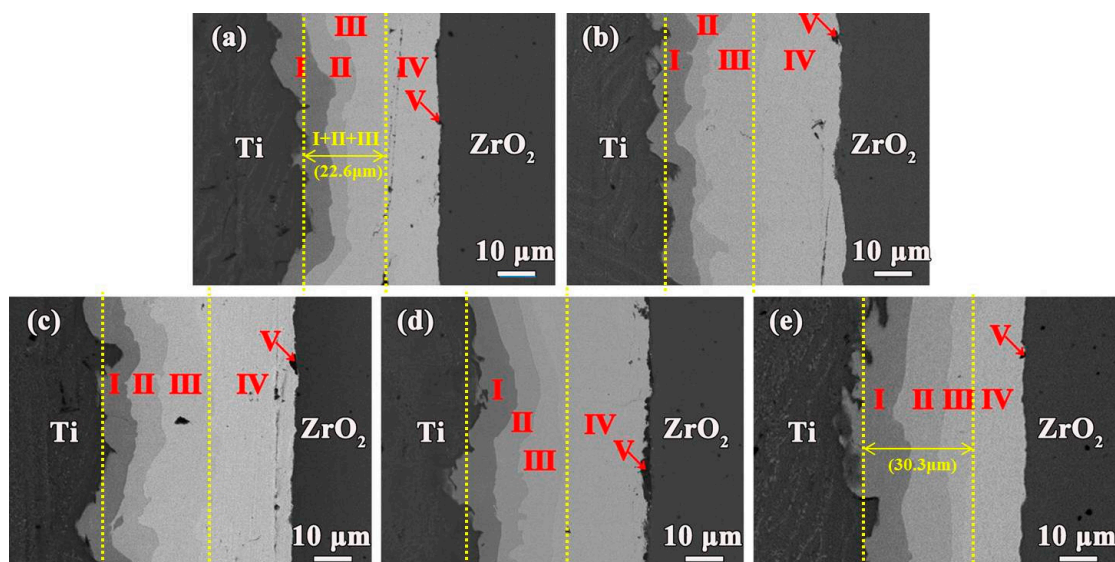

Figure 6. Microstructure of the titanium/Au/ZrO_2 joint brazed at 1150 °C for different holding times: (**a**) 5 min, (**b**) 10 min, (**c**) 15 min, (**d**) 20 min and (**e**) 30 min.

In summary, the effects of the brazing parameters on the microstructural evolution of the joints can be summarized as follows: when the brazing temperature exceeded the melting point of the Au foil, the Au foil started to melt and spread on the surface of the titanium substrate. Meanwhile, Ti dissolved

and diffused to the molten Au which was driven by the concentration gradient of Ti. On the one hand, Ti reacted with Au to form Ti–Au IMCs. In the cooling process, Ti_3Au, $TiAu$, $TiAu_2$ and $TiAu_4$ layers formed simultaneously in the brazing seam due to the decreasing concentration gradient of Ti. With the temperature increasing, the diffusion of Ti and Au was facilitated, and the concentration gradient of Ti grew. Therefore, the thickness of the $Ti_3Au + TiAu + TiAu_2$ layer increased gradually. However, with the brazing temperature increasing further, Ti–Au IMC layers prevented the further interdiffusion of Ti and Au atoms, which resulted in an indiscernible change in the thickness of $Ti_3Au + TiAu + TiAu_2$ layers. Similar to the effect of the brazing temperature, with a longer holding time, the diffusion of Ti and Au atoms was more sufficient, and the thickness of the $Ti_3Au + TiAu + TiAu_2$ layer increased. On the other hand, redundant Ti diffused to the ZrO_2 ceramic side crossing the brazing seam and accumulated on the surface of the ZrO_2 ceramic. Active Ti could partially capture oxygen from ZrO_2 to form a TiO compound. When the brazing temperature was low, the diffusion speed of the Ti atoms was slow and the number of Ti atoms that diffused to the ZrO_2 surface was limited. Therefore, the TiO layer was too thin to be observed by SEM. With an increase in temperature, a more sufficient diffusion of Ti atoms to the ZrO_2 surface occurred, which then accumulated on the ZrO_2 surface and reacted with the O atoms from ZrO_2. Therefore, the thickness of the TiO layers increased gradually. However, with a longer holding time, the Ti-Au IMC layers hindered the diffusion of more Ti atoms to ZrO_2. Thus, the TiO layer displayed no significant change, except for a slight increase in thickness.

3.3. Mechanical Properties and Fracture Morphology of Titanium/Au/ZrO$_2$ Joint

To evaluate the mechanical properties of the brazed joints, shear tests at room temperature were carried out. Figure 7a,b illustrated the effect of the brazing temperature and holding time on the average shear strength of titanium/Au/ZrO$_2$ joints, respectively. It can be seen clearly that both temperature and holding time influenced the shear strength significantly. The shear strength improved with the increase in brazing temperature and holding time, until the optimal shear strength of ~35.0 MPa was reached at 1150 °C for 10 min, and then decreased.
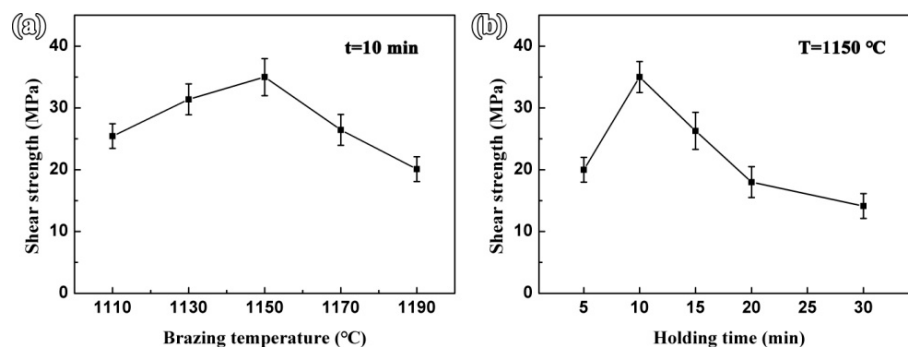

Figure 7. Effect of brazing parameters on shear strength of titanium/Au/ZrO$_2$ joint. (**a**) Brazing temperature and (**b**) holding time.

In order to further investigate the fracture mechanisms of the joints after the shear test, the fracture paths and their magnified fractographs at different brazing temperature and holding times are shown in Figure 8(a1–a2,b1–b2,c1–c2). Moreover, the corresponding XRD spectra (ZrO_2: PDF#01-088-1007, $TiAu_2$: PDF#00-029-0651 and $TiAu_4$: PDF#04-004-9165) on the ZrO_2 side are illustrated in Figure 8(a3,b3,c3). When the joints were brazed at a low temperature or for a short holding time—for example, 1110 °C/10 min—the diffusion of Ti and Au atoms was slow and insufficient. Thus, only a limited number of Ti atoms diffused to the ZrO_2 surface and reacted with ZrO_2 to form a TiO layer. As a result, the TiO layer was too thin, resulting in weak metallurgical bonding between ZrO_2 and the brazing alloy. As a result, cracks initiated in the ZrO_2/$TiAu_4$ interface and propagated to the brazing seam, mainly causing cracks on the $TiAu_4$/$TiAu_2$ (Zone IV/III) interface, as shown in Figure 8(a1–a2). The corresponding XRD spectrum on the ZrO_2 side in Figure 8(a3) mainly contained

$TiAu_4$ and $TiAu_2$ phases, which further proves the above analysis. With the temperature increasing, the diffusion of Ti and Au atoms accelerated and more Ti atoms accumulated on the ZrO_2 surface, forming a thicker and more continuous TiO layer in order to achieve better metallurgical bonding on the ZrO_2/brazing seam interface. In this case, the shear strength increased gradually. Figure 8(b1–b2) shows the crack path and fractography obtained at 1150 °C for 10 min. The thickness of the TiO layer was the most moderate and the joint achieved the maximum shear strength. The joints mainly cracked on the brazing seam. Combined with the XRD spectrum in Figure 8(b3), it can be concluded that the fracture path was located on the $TiAu_4$/$TiAu_2$ interface. With the brazing temperature and holding time further increasing, the TiO layer became thicker and the residual stress between ZrO_2 and the brazing seam increased. As a result, the joints mainly cracked on the brazing seam and the ZrO_2/$TiAu_4$ interface, as shown in Figure 8(c1–c3) for the joint brazed at 1150 °C for 30min. Based on the above analysis, it can be deduced that the formation and proper thickness of the TiO layer was crucial to the shear strength of the joints.
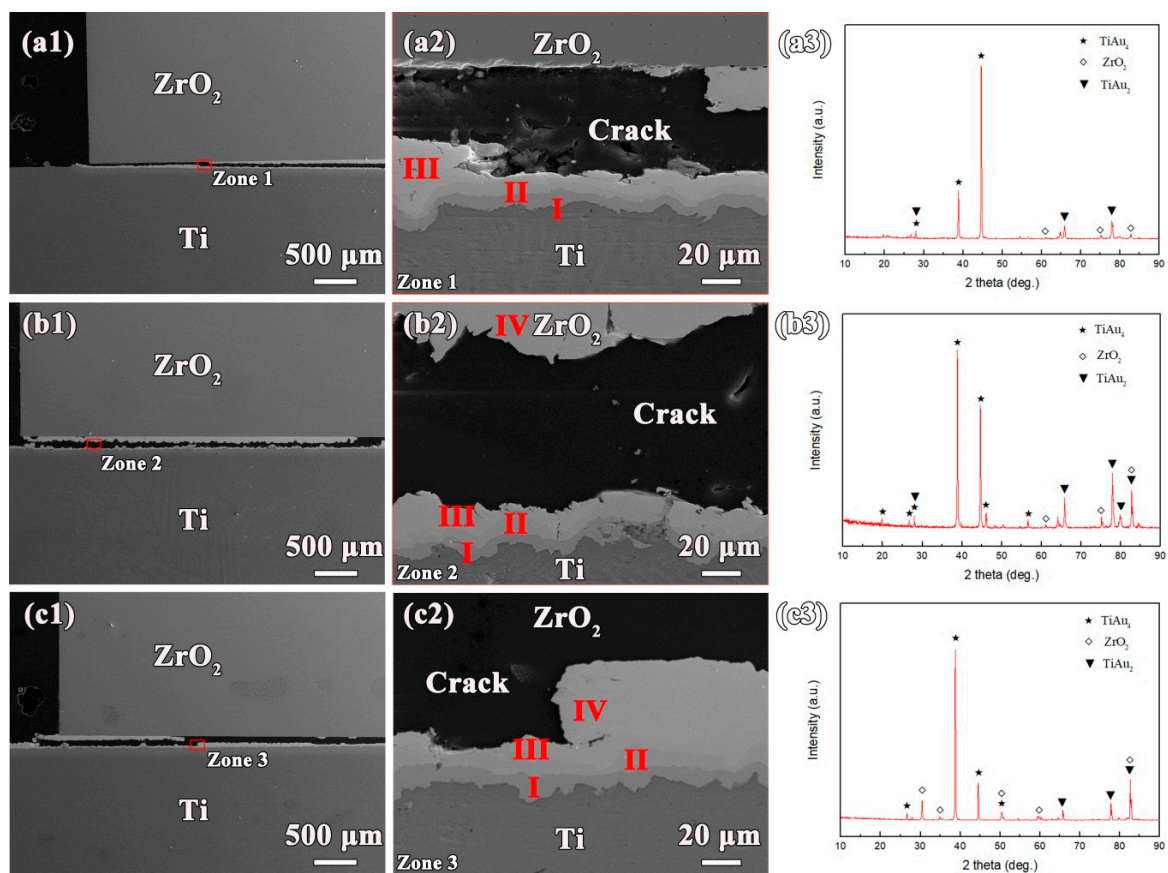

Figure 8. Fracture paths, high-magnification fractographs and XRD patterns of titanium/Au/ ZrO_2 joints brazed at different parameters after the shear test. (**a1–a3**) 1110 °C for 10 min, (**b1–b3**) 1150 °C for 10 min, and (**c1–c3**) 1150 °C for 30 min.

4. Conclusions

In this study, the reliable bonding of biomedical titanium/ZrO_2 was successfully achieved using Au foil. The typical interfacial microstructure of the brazed joint was characterized. The effects of brazing temperature and holding time on the interfacial microstructure and mechanical properties of the joints were investigated in detail. In conclusion:

(1) Ti_3Au, TiAu, $TiAu_2$, $TiAu_4$ and TiO phases were formed in the brazed joint. The typical interfacial microstructure of the titanium/Au/ZrO_2 joint was titanium/Ti_3Au layer/TiAu layer/$TiAu_2$

layer/TiAu$_4$ layer/TiO layer/ZrO$_2$ ceramic. The thicknesses of these layers, on average, were ~4.8 µm, 5.3 µm, 14.2 µm and 10.2 µm;

(2) The brazing temperature and holding time had significant effects on the interfacial microstructure and mechanical properties of the brazed joints. With a higher brazing temperature or a longer holding time, the diffusion of Ti and Au was accelerated, and the thickness of the Ti$_3$Au + TiAu + TiAu$_2$ layers increased gradually. The TiO layer thickened gradually and promoted metallurgical bonding between the brazing alloy and the ZrO$_2$ ceramic;

(3) The joint brazed at 1150 °C for 10 min had an optimal shear strength of ~35.0 MPa, and a TiO layer with a modest thickness. A crack was initiated and propagated along the interface of the TiAu$_2$ and TiAu$_4$ reaction layers.

Author Contributions: Conceptualization, X.S. and W.L.; formal analysis, Y.L.; funding acquisition, H.B. and X.S.; investigation, Y.L., W.F. and H.N.; project administration, J.F.; resources, H.N.; supervision, H.B. and J.F.; validation, W.F.; visualization, W.F.; writing—original draft, Y.L.; writing—review & editing, all authors. All authors have read and agreed to the published version of the manuscript.

References

1. Xu, L.; Li, J.; Xu, X.; Lei, X.; Zhang, K.; Wu, C.; Zhang, Z.; Shi, X.; Wang, X.; Ding, J. A Novel Cytocompatibility Strengthening Strategy of Ultrafine-Grained Pure Titanium. *ACS Appl. Mater. Interfaces* **2019**, *11*, 47680–47694. [CrossRef]

2. Kumar, D.D.; Kaliaraj, G.S. Multifunctional zirconium nitride/copper multilayer coatings on medical grade 316L SS and titanium substrates for biomedical applications. *J. Mech. Behav. Biomed. Mater.* **2018**, *77*, 106–115. [CrossRef]

3. Gao, C.; Li, C.; Wang, C.; Qin, Y.; Wang, Z.; Yang, F.; Liu, H.; Chang, F.; Wang, J. Advances in the induction of osteogenesis by zinc surface modification based on titanium alloy substrates for medical implants. *J. Alloys Compd.* **2017**, *726*, 1072–1084. [CrossRef]

4. Kaur, M.; Singh, K. Review on titanium and titanium based alloys as biomaterials for orthopaedic applications. *Mater. Sci. Eng. C Mater. Biol. Appl.* **2019**, *102*, 844–862. [CrossRef] [PubMed]

5. Mishnaevsky, L.; Levashov, E.; Valiev, R.Z.; Segurado, J.; Sabirov, I.; Enikeev, N.; Prokoshkin, S.; Solov'yov, A.V.; Korotitskiy, A.; Gutmanas, E.; et al. Nanostructured titanium-based materials for medical implants: Modeling and development. *Mater. Sci. Eng. R Rep.* **2014**, *81*, 1–19. [CrossRef]

6. Korobkova, A.; Kazakbiev, A.; Zhukova, Y.; Sheremetyev, V.; Dubinskiy, S.; Filonov, M. Surface treatment of bulk and porous materials based on superelastic titanium alloys for medical implants. *Mater. Today Proc.* **2017**, *4*, 4664–4669. [CrossRef]

7. Liu, L.; Xu, J.; Jiang, S. Nanocrystalline β-Ta Coating Enhances the Longevity and Bioactivity of Medical Titanium Alloys. *Metals* **2016**, *6*, 221. [CrossRef]

8. Reck, A.; Zeuner, A.T.; Zimmermann, M. Fatigue Behavior of Non-Optimized Laser-Cut Medical Grade Ti-6Al-4V-ELI Sheets and the Effects of Mechanical Post-Processing. *Metals* **2019**, *9*, 843. [CrossRef]

9. Ayoub, G.; Veljovic, D.; Zebic, M.L.; Miletic, V.; Palcevskis, E.; Petrovic, R.; Janackovic, D. Composite nanostructured hydroxyapatite/yttrium stabilized zirconia dental inserts–The processing and application as dentin substitutes. *Ceram. Int.* **2018**, *44*, 18200–18208. [CrossRef]

10. Marques, A.; Miranda, G.; Faria, D.; Pinto, P.; Silva, F.; Carvalho, O. Novel design of low modulus high strength zirconia scaffolds for biomedical applications. *J. Mech. Behav. Biomed. Mater.* **2019**, *97*, 375–384. [CrossRef]

11. Dandoulaki, C.; Rigos, A.E.; Kontonasaki, E.; Karagiannis, V.; Kokoti, M.; Theodorou, G.S.; Papadopoulou, L.; Koidis, P. In vitro evaluation of the shear bond strength and bioactivity of a bioceramic cement for bonding monolithic zirconia. *J. Prosthet. Dent.* **2019**, *122*, e1–e167. [CrossRef] [PubMed]

12. Stefanic, M.; Kosmač, T. β-TCP coatings on zirconia bioceramics: The importance of heating temperature on the bond strength and the substrate/coating interface. *J. Eur. Ceram. Soc.* **2018**, *38*, 5264–5269. [CrossRef]

13. Volceanov, E.; Popa, C.G.; Volceanov, A.; Ciuca, S. Chemical stability in artificial saliva of zirconia bioceramics. *Rev. Romana Mater. Rom. J. Mater.* **2019**, *49*, 313–321.

14. Cantner, F.; Cacaci, C.; Mucke, T.; Randelzhofer, P.; Hajto, J.; Beuer, F. Clinical performance of tooth- or implant-supported veneered zirconia single crowns: 42-month results. *Clin. Oral Investig.* **2019**, *23*, 4301–4309. [CrossRef]

15. Parchanska-Kowalik, M.; Wolowiec-Korecka, E.; Klimek, L. Effect of chemical surface treatment of titanium on its bond with dental ceramics. *J. Prosthet. Dent.* **2018**, *120*, 470–475. [CrossRef]

16. Smorygo, O.; Kim, J.S.; Kim, M.D.; Eom, T.G. Evolution of the interlayer microstructure and the fracture modes of the zirconia/Cu–Ag–Ti filler/Ti active brazing joints. *Mater. Lett.* **2007**, *61*, 613–616. [CrossRef]

17. Yadav, J.S.; Dabas, N.; Bhargava, A.; Malhotra, P.; Yadav, B.; Sehgal, M. Comparing two intraoral porcelain repair systems for shear bond strength in repaired cohesive and adhesive fractures, for porcelain-fused-to-metal restorations: An in vitro study. *J. Indian Prosthodont. Soc.* **2019**, *19*, 362–368. [CrossRef]

18. Haselton, D.R.; Diaz-Arnold, A.M.; Dunne, J.T., Jr. Shear bond strengths of 2 intraoral porcelain repair systems to porcelain or metal substrates. *J. Prosthet. Dentistry* **2001**, *86*, 526–531. [CrossRef]

19. Han, X.; Sawada, T.; Schille, C.; Schweizer, E.; Scheideler, L.; Geis-Gerstorfer, J.; Rupp, F.; Spintzyk, S. Comparative Analysis of Mechanical Properties and Metal-Ceramic Bond Strength of Co-Cr Dental Alloy Fabricated by Different Manufacturing Processes. *Materials* **2018**, *11*, 1801. [CrossRef]

20. Zhou, Y.; Wei, W.; Yan, J.; Liu, W.; Li, N.; Li, H.; Xu, S. Microstructures and metal-ceramic bond properties of Co-Cr biomedical alloys fabricated by selective laser melting and casting. *Mater. Sci. Eng. A* **2019**, *759*, 594–602. [CrossRef]

21. Li, C.; Huang, C.; Chen, L.; Si, X.; Chen, Z.; Qi, J.; Huang, Y.; Feng, J.; Cao, J. Microstructure and mechanical properties of the SiC/Nb joint brazed using AgCuTi+B_4C composite filler metal. *Int. J. Refract. Met. Hard Mater.* **2019**, *85*, 105049. [CrossRef]

22. Way, M.; Willingham, J.; Goodall, R. Brazing filler metals. *Int. Mater. Rev.* **2020**, *65*, 257–285. [CrossRef]

23. Hu, S.P.; Hu, T.Y.; Lei, Y.Z.; Song, X.G.; Liu, D.; Cao, J.; Tang, D.Y. Microstructural evolution and mechanical properties of vacuum brazed Ti_2AlNb alloy and Ti60 alloy with Cu75Pt filler metal. *Vacuum* **2018**, *152*, 340–346. [CrossRef]

24. Sharma, A.; Kee, S.H.; Jung, F.; Heo, Y.; Jung, J.P. Compressive Strength Evaluation in Brazed ZrO_2/Ti6Al$_4$V Joints Using Finite Element Analysis. *J. Mater. Eng. Perform.* **2016**, *25*, 1722–1728. [CrossRef]

25. Sharma, A.; Ahn, B. Brazeability, Microstructure, and Joint Characteristics of ZrO_2/Ti-6Al-4V Brazed by Ag-Cu-Ti Filler Reinforced with Cerium Oxide Nanoparticles. *Adv. Mater. Sci. Eng.* **2019**, *2019*, 1–11. [CrossRef]

26. Fu, W.; Song, X.; Passerone, A.; Hu, S.; Bian, H.; Zhao, Y.; Wang, M.; Valenza, F. Interactions, joining and microstructure of Sn-Ti/ZrO_2 system. *J. Eur. Ceram. Soc.* **2019**, *39*, 1525–1531. [CrossRef]

27. Bian, H.; Fu, W.; Lei, Y.Z.; Song, X.G.; Liu, D.; Cao, J.; Feng, J.C. Wetting and low temperature bonding of zirconia metallized with Sn0.3Ag0.7Cu-Ti alloys. *Ceram. Int.* **2018**, *44*, 11456–11465. [CrossRef]

28. Bian, H.; Zhou, Y.; Song, X.; Hu, S.; Shi, B.; Kang, J.; Feng, J. Reactive wetting and interfacial characterization of ZrO_2 by SnAgCu-Ti alloy. *Ceram. Int.* **2019**, *45*, 6730–6737. [CrossRef]

29. Feng, J.; Dai, X.; Wang, D.; Li, R.; Cao, J. Microstructure evolution and mechanical properties of ZrO_2/TiAl joints vacuum brazed by Ag–Cu filler metal. *Mater. Sci. Eng. A* **2015**, *639*, 739–746. [CrossRef]

30. Dai, X.; Cao, J.; Liu, J.; Wang, D.; Feng, J. Interfacial reaction behavior and mechanical characterization of ZrO_2/TC4 joint brazed by Ag–Cu filler metal. *Mater. Sci. Eng. A* **2015**, *646*, 182–189. [CrossRef]

31. Jain, P.K. Gold Nanoparticles for Physics, Chemistry, and Biology. Edited by Catherine Louis and Olivier Pluchery. *Angew. Chem. Int. Ed.* **2014**, *53*, 1197. [CrossRef]

32. Manickam, P.; Vashist, A.; Madhu, S.; Sadasivam, M.; Sakthivel, A.; Kaushik, A.; Nair, M. Gold nanocubes embedded biocompatible hybrid hydrogels for electrochemical detection of H_2O_2. *Bioelectrochemistry* **2020**, *131*, 107373. [CrossRef] [PubMed]

33. Iram, F.; Iqbal, M.S.; Khan, I.U.; Rasheed, R.; Khalid, A.; Khalid, M.; Aftab, S.; Shakoori, A.R. Synthesis and Biodistribution Study of Biocompatible (198)Au Nanoparticles by use of Arabinoxylan as Reducing and Stabilizing Agent. *Biol. Trace Elem. Res.* **2020**, *193*, 282–293. [CrossRef] [PubMed]

34. Shuai, H.L.; Wu, X.; Huang, K.J.; Zhai, Z.B. Ultrasensitive electrochemical biosensing platform based on spherical silicon dioxide/molybdenum selenide nanohybrids and triggered Hybridization Chain Reaction. *Biosens. Bioelectron.* **2017**, *94*, 616–625. [CrossRef]

35. Manohar, N.; Reynoso, F.J.; Diagaradjane, P.; Krishnan, S.; Cho, S.H. Quantitative imaging of gold nanoparticle distribution in a tumor-bearing mouse using benchtop x-ray fluorescence computed tomography. *Sci. Rep.* **2016**, *6*, 22079. [CrossRef]

36. Chen, Z.; Meng, H.; Xing, G.; Chen, C.; Zhao, Y.; Jia, G.; Wang, T.; Yuan, H.; Ye, C.; Zhao, F.; et al. Acute toxicological effects of copper nanoparticles in vivo. *Toxicol. Lett.* **2006**, *163*, 109–120. [CrossRef]

37. Murray, J.L. The Au-Ti (Gold-Titanium) system. *Bull. Alloy. Phase Diagr.* **1983**, *4*, 278–283. [CrossRef]

38. Bian, H.; Song, X.; Hu, S.; Lei, Y.; Jiao, Y.; Duan, S.; Feng, J.; Long, W. Microstructure Evolution and Mechanical Properties of Titanium/Alumina Brazed Joints for Medical Implants. *Metals* **2019**, *9*, 644. [CrossRef]

39. Lin, K.F.; Lin, C.C. Interfacial reactions between zirconia and titanium. *Scr. Mater.* **1998**, *39*, 1333–1338. [CrossRef]

40. Hanson, W.B.; Ironside, K.I.; Fernie, J.A. Active metal brazing of zirconia. *Acta Mater.* **2000**, *48*, 4673–4676. [CrossRef]

41. Zhu, J.; Kamiya, A.; Yamada, T.; Shi, W.; Naganuma, K.; Mukai, K. Surface tension, wettability and reactivity of molten titanium in Ti/yttria-stabilized zirconia system. *Mater. Sci. Eng. A* **2002**, *327*, 117–127. [CrossRef]

42. Wang, N.; Wang, D.P.; Yang, Z.W.; Wang, Y. Interfacial microstructure and mechanical properties of zirconia ceramic and niobium joints vacuum brazed with two Ag-based active filler metals. *Ceram. Int.* **2016**, *42*, 12815–12824. [CrossRef]

43. Zhang, Q.; Wang, J.; Zheng, K.; Lu, Y.; Yang, H. Microstructure evolution and mechanical properties of ZrO_2/ZrO_2 joints brazed with Ni–Ti filler metal. *Mater. Res. Express* **2019**, *6*, 126547. [CrossRef]